*Transactions of the 17th International Conference on Structural Mechanics in Reactor Technology (***SMiRT 17***)*
***Prague, Czech Republic, August 17 –22, 2003***

***Paper # B03-3***

# Generation Possibilities of Lower Frequency Components in Fluid Temperature Fluctuations Related to Thermal Striping Phenomena

Toshiharu MURAMATSU

*Japan Nuclear Cycle Development Institute, Japan*

**ABSTRACT**

Fluid-structure thermal interaction phenomena characterized by stationary random temperature fluctuations, namely thermal striping are observed in the downstream region of a T-junction piping system of liquid metal fast reactor (LMFR). Therefore the piping walls located in the downstream region must be protected against the stationary random thermal process which might induce high-cycle fatigue. This paper investigates generation possibilities of damageable lower frequency components in fluid temperature fluctuations at the downstream region of T-junction piping systems based on the results from a fundamental water experiment and numerical simulations. In the fundamental water experiment, it was confirmed that an arched vortex streak with the lower frequency components are generated in the condition of $\beta = 0.8$, which is defined as the ratio of main pipe flow velocity to branch pipe flow velocity ($\equiv$ Vm/Vb). On the one hand, a continuous arched vortex streak with the lower frequency components of interest was evaluated with a thermohydraulic numerical simulation in the condition of $\beta = 0.8$.

From the results, it was confirmed that special attentions should be paid to the arched vortex generations with lower frequency components of fluid temperature fluctuations, which might induced high-cycle thermal fatigue for the design of T-junction systems.

**KEYWORDS:** computational fluid dynamics, turbulence flows, computer code, thermal striping, temperature fluctuation, nuclear power plant, LMFBR type reactors, thermal fatigue, T-junction pipe, mixing tee, arched vortex

## 1. INTRODUCTION

Thermal striping phenomena characterized by stationary random temperature fluctuations are observed in the region immediately above the core exit of LMFRs due to the interactions of cold sodium flowing out of a control rod (C/R) assembly and hot sodium flowing out of adjacent fuel assemblies (F/As). The same phenomena occur in various positions, such as a mixing tee [1], [2], [3], a combining junction pipe, *etc*. of nuclear power plants including the LMFRs. Therefore, the in-vessel components located in the core outlet region, such as upper core structure (UCS), flow guide tube, C/R upper guide tube, and so forth, must be protected against the stationary random thermal process which might induce high-cycle fatigue. In this regard, Alloy 718 is generally adopted as a coating material to protect these components against fatigue. Most evaluations of this kind have so far been based on 1:1 or other scale-model experiments using sodium in Japan. In practice, thermal striping conditions in a Japanese prototype LMFR were evaluated through 1:1 scale model experiments in sodium. In such a conventional approach, an increase in the cost and time to perform the experiments cannot be avoided. Furthermore, in sodium experiments, we often encounter technical difficulties in obtaining adequate amounts and quality of data. For these reasons, establishment of numerical evaluation methods is desirable in support of the experimental approach to understanding fluid temperature fluctuation phenomena. From this viewpoint, author is developing an evaluation system for the thermal striping phenomena based on numerical methods consisting of four thermohydraulics computer programs AQUA [4], [5], DINUS-3 [6], [7], THEMIS [8] and BEMSET [9] and of two thermomechanics computer programs FINAS [10] and CANIS [11].

This paper describes generation possibilities of damageable lower frequency components in fluid temperature fluctuations at the downstream region of T-junction piping systems based on the results from a fundamental water experiment and numerical simulations with the recognition, which is frequent occurrences of the thermal fatigue damage at the T-junction piping systems of actual nuclear power plants, for example, French prototype FBR Phenix in 1992 (see Appendix), French advanced PWR Civaux in 1998, Japanese PWR Turuga unit-2 in 1999, *etc*., as a background.

## 2. NUMERICAL SIMULATION METHODS

Figure 1 shows an evaluation system for the thermal striping phenomena based on numerical methods developed at Japan Nuclear Cycle Development Institute (JNC). The system verified well through sodium experiments [12], [13] consists of six major parts.

Very briefly, the major parts are:

1. to evaluate the spatial intensity distribution of the fluid temperature fluctuations containing lower frequency components with the AQUA code;
2. to evaluate the time-series data of the fluid temperature fluctuations having both the lower and higher frequencies with the DINUS-3 code;
3. to evaluate non-stationary heat transfer coefficients between fluid and structure with the THEMIS code;
4. to evaluate the thermal response characteristics for structures with the BEMSET code;
5. to evaluate the thermal stress distributions in structures with the FINAS code; and
6. to evaluate the crack propagation characteristics of structures with the CANIS code.

Table 1 shows main features of computer programs for thermal striping evaluations.

## 3. FUNDAMENTAL WATER EXPERIMENT

### 3. 1 Outline of the Experiment

A fundamental water experiment was carried out at Hiroshima university, Japan [14] in the framework of a cooperative study with JNC to investigate turbulent mixing mechanism in the downstream region of a T-junction piping system.

Figure 2 shows an outline of the water experimental apparatus and arrangement of attached components. The experimental apparatus consisted of a main pipe, a branch pipe, two pumps, dye injection lines, and four water tanks. The T-junction piping system was modeled by a rectangular main duct (40 mm x 40 mm x 2500 mm) and a cylindrical branch pipe of diameter 9 mm. Then the diameter ratio $\alpha$ ($\equiv$ Dm / Db) was kept constant of 4.44 (= 40.0 mm / 9.0 mm). In the experiment, dye tracer was injected into the test section and the flow fields and mixing process were visualized by a high-speed camera system under various test conditions with regard to the flow velocity ratio $\beta$ (Vm / Vb ~ 3.0). It is noted that, in the experiment at Hiroshima university, no temperature field was measured due to isothermal test conditions of a room temperature. Furthermore, no bend was considered in upstream region of the T-junction piping system due to the first step

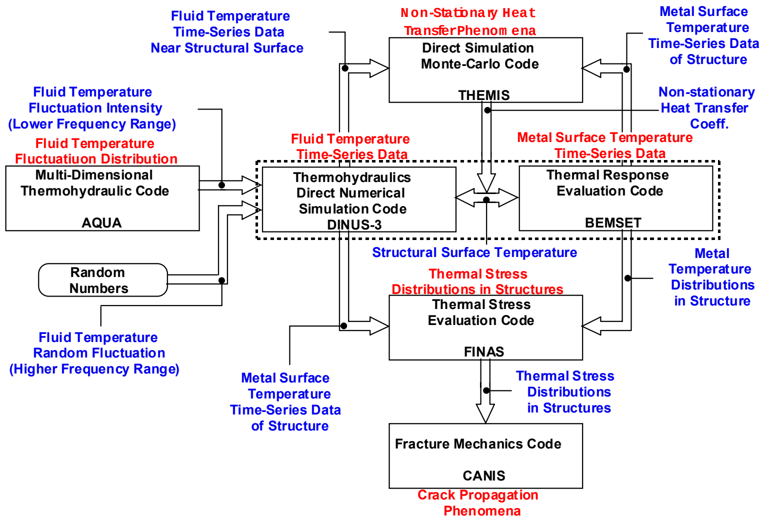


Fig. 1 Evaluation system for the thermal striping based on numerical methods

Table 1 Main features of computer programs

| Items | AQUA | DINUS-3 | THEMIS | BEMSET | FINAS | CANIS |
|---|---|---|---|---|---|---|
| 1. Basic Equation or Theory | Time-Averaged N-S Eq. | Instantaneous N-S Eq. | Boltzmann Eq. | Thermoelastic Linealized Eq. | Thermoelastic Theory | Linear Fracture Mechanics Theory |
| 2. Mathematical Models | | | | | | |
| Descretization | FDM | FDM | None | BEM | FEM | |
| Solution Algorithm | Modified ICE | Leap-Frog | DSMC | | Pred. / Corr. | Weight Function |
| Approx. Method for Convection Terms | 2nd Order QUICK | 3rd Order Upwind | | | | |
| Boundary Elements | | | | Rectangular | | |
| Matrix Solver | ICCG | ICCG | | Direct | Direct | |
| Coordinate System | x-y-z / r-θ-z | x-y-z / r-θ-z | x-y-z / r-θ-z | x-y-z / r-θ-z | Boundary Fit | |
| 3. Physical Models | | | | | | |
| Turbulence Model | ASM / RSM | None | | | | |
| Molecular Model | | | Monoatomic Sphere | | | |
| Collision Model | | | Bird's Model | | | |
| Material Model | | | | | Thermoelastic Constitutive Model | |
| Fracture Mechanics | | | | | | Stress Intensity Fact. |
| 4. Others | | | | | | |
| Numerical Stabilizer | Fuzzy Controller | Fuzzy Controller | | | | |

Note : FDM (Finite Difference Method), ICE (Incompressible Continuous Eulerian), QUICK (Quadratic Upstream Interpolation for Convective Kinematics), ICCG (Incomplete Choleski Conjugate Gradient), ASM (Algebraic Stress turbulence Model), RSM (Reynolds Stress turbulence Model), DSMC (Direct Simulation Monte Carlo), BEM (Boundary Element Method), FEM (Finite Difference Method)

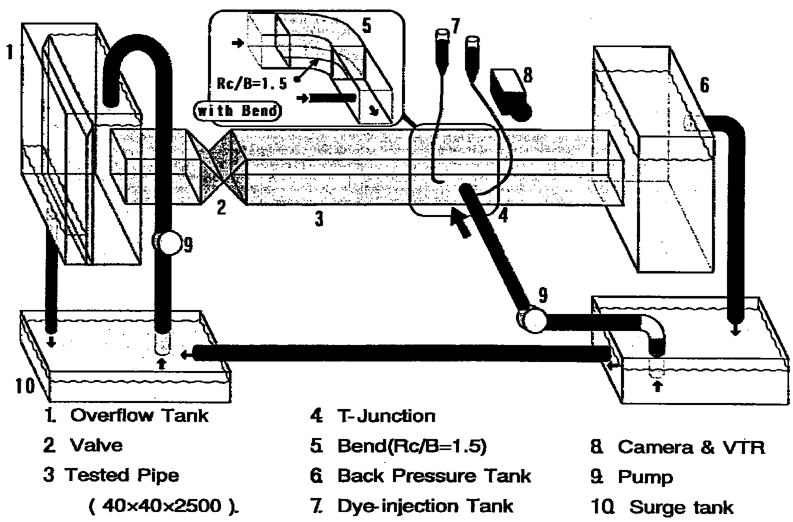


Fig. 2 Apparatus of the fundamental water experiment for T-junction piping system

of the water experiment series.

3. 2 Outline of the Experimental Results

Visualized flow patterns were classified into three categories: i.e., (1) impinging jet flow, (2) deflection jet flow and (3) adhesion jet flow. These visualized flow patterns were indicated in Fig. 3. As shown in Fig. 9 (b), an arched vortex streak was observed under the condition of the deflection jet pattern. This is due to intermittent vortex shedding from the front of the branch pipe jet induced by the main duct flows.

Figure 4 illustrates a flow pattern map with respect to the inner diameter ratio $\alpha$, the flow velocity ratio $\beta$ and Reynolds number (Re) based on the rectangular main duct. In the figure, the experimental results were formulated into the following equations as a function of $\alpha$, $\beta$ and Re from viewpoint of an universal uses.

$$G_1 = 20.8\ \alpha \beta^{1.26}\ Re^{-0.737} \tag{1}$$

$$G_2 = 2.01\ \alpha \beta^{1.86}\ Re^{-0.138} \tag{2}$$

The figure indicates that the range appearing the deflection jet pattern is limited for the condition of $G_1 < 1.0$ and $G_2 > 1.0$. These facts, however, suggest to us that the there is the possibility of the arched vortex generations in engineering problems using various conditions of $\alpha$, $\beta$ and Re.

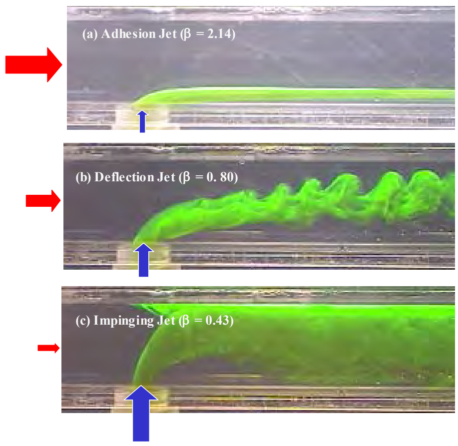


Fig. 3 Measured typical flow patterns under various $\beta$ conditions.

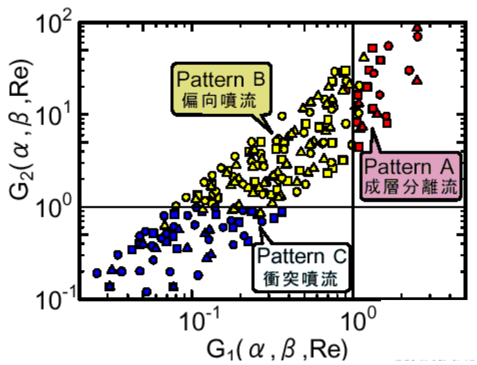


Fig. 4 Flow pattern map based on the water experimental results

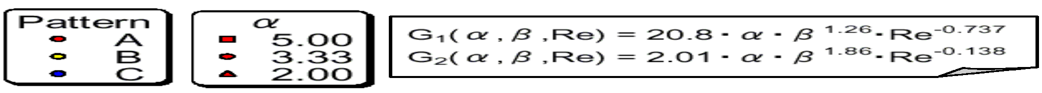


## 4. NUMERICAL SIMULATIONS

4. 1 Calculation and Boundary Conditions

Calculations were carried out with a quasi-direct numerical simulation code DINUS-3 solving instantaneous Navier-Stokes equations for the total of five cases, i.e., ($\beta$, Re) = (0.2, 600) for the impinging jet condition; (1.0, 600), (1.0, 1050) and (3.0, 5000) for the deflection jet condition; and (2.6, 600) for the adhesion jet condition. Figure 5 illustrate a computational domain (x-y-z : 98 mm x 40 mm x 40 mm). Computational cells which contained no internal solid structure numbered up to 1254400 with uniform meshes of 0.5 mm.

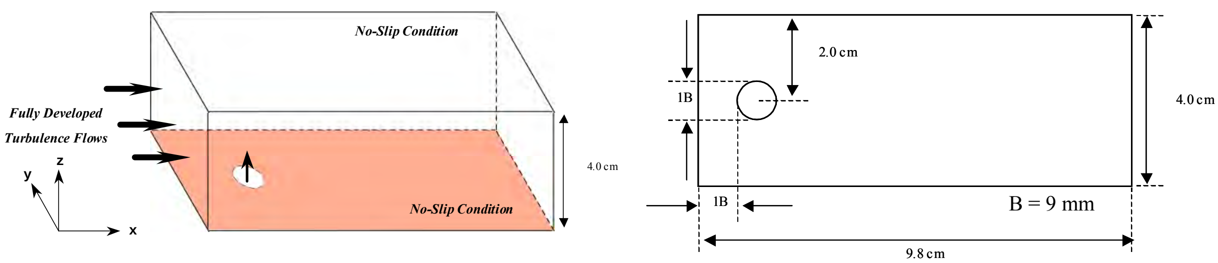


[ perspective view ] [ x-y plane view ]

Fig. 5 Computational domain for DINUS-3 analyses

The no-slip condition for the velocity components and adiabatic condition were assumed on the solid surfaces. It is noted here that we did not employ any wall functions, because we utilized a direct numerical simulation code. Logarithmic velocity distributions of turbulence flows were set to the inlet plane as a boundary condition.

Given all thermohydraulic data at t=0, a transient was calculated up to a quasi-steady-state level [$(\phi^{n+1} - \phi^{n}) / \phi^{n} = 10^{-4}$] using a time marching method. Then a restart transient calculation storing calculated time-series data was continued up to a 6-s simulation time with a constant time interval of 10 ms.

### 4. 2 Calculated Results

Figure 6 shows calculated instantaneous distributions for vorticities and stream lines on the x-z plane at J=30. As shown in the figures, although we were not able to make a direct quantitative comparison of the vorticity distributions with the experimental results, we consider that qualitative agreement between the experiment and calculation was obtained with respect to the flow pattern in the downstream region.

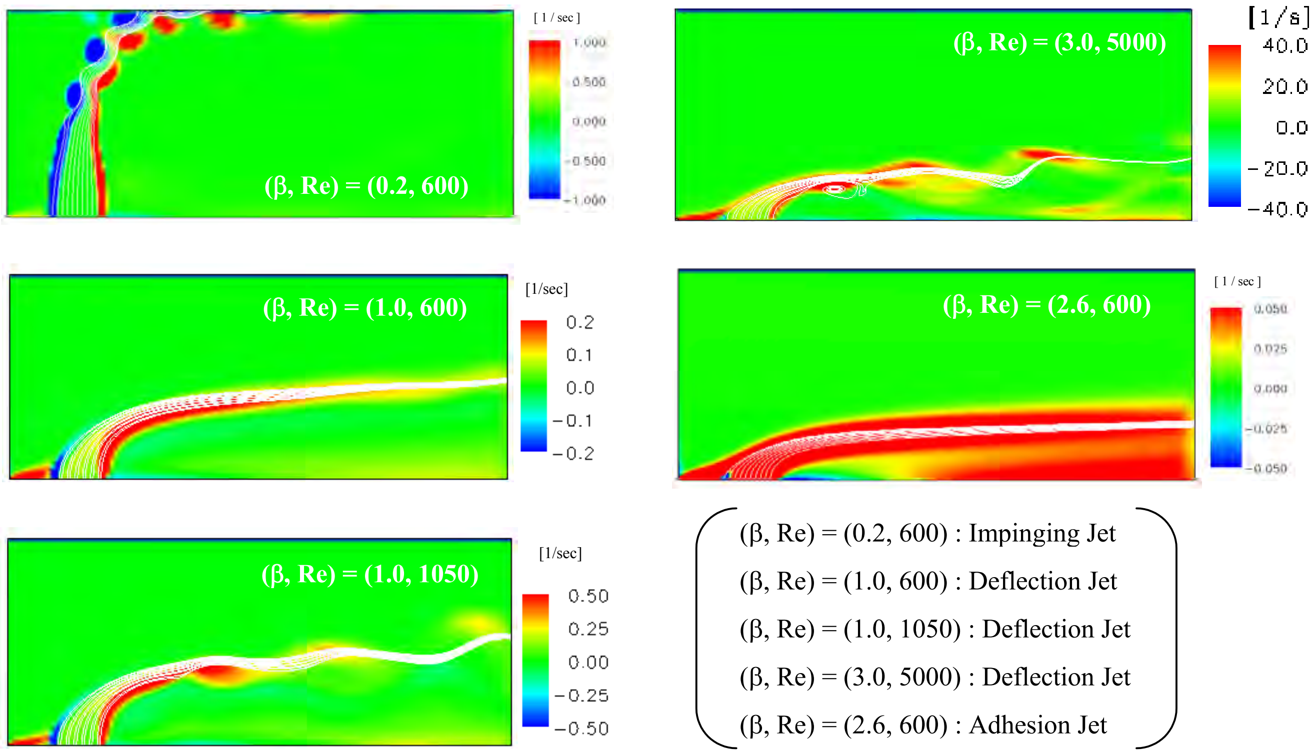


Fig. 6 Instantaneous distributions for vorticities and stream lines for various jet conditions

## 5. DISCUSSIONS

Iso-surface transients of a cross flow velocity components defined by the following equation are illustrated in Fig. 7 for the case of the deflection jet condition (($\beta$, Re) = (1.0, 600)).

$$Vc = (V^2 + W^2)^{0.5} \qquad (3)$$

where

- Vc : cross flow velocity,
- V : velocity component in y-direction,
- W : velocity component in z-direction.

As shown in Fig. 7, arched vortexes (shown by a red line circle) composed of generation, shedding and movement from the front of the branch pipe jet were evaluated in this deflection jet condition.

To understand the arched vortex structures, vorticity distributions were superimposed on an instantaneous iso-surface distributions of the cross flow velocity components as shown in Fig. 8. The rotating directions of the vorticities around the arched vortexes were to the outside from the inside of the arched vortexes. This supports phenomeno- logically that the arched vortex was caused by vortex separation from the front of the branch pipe jet.

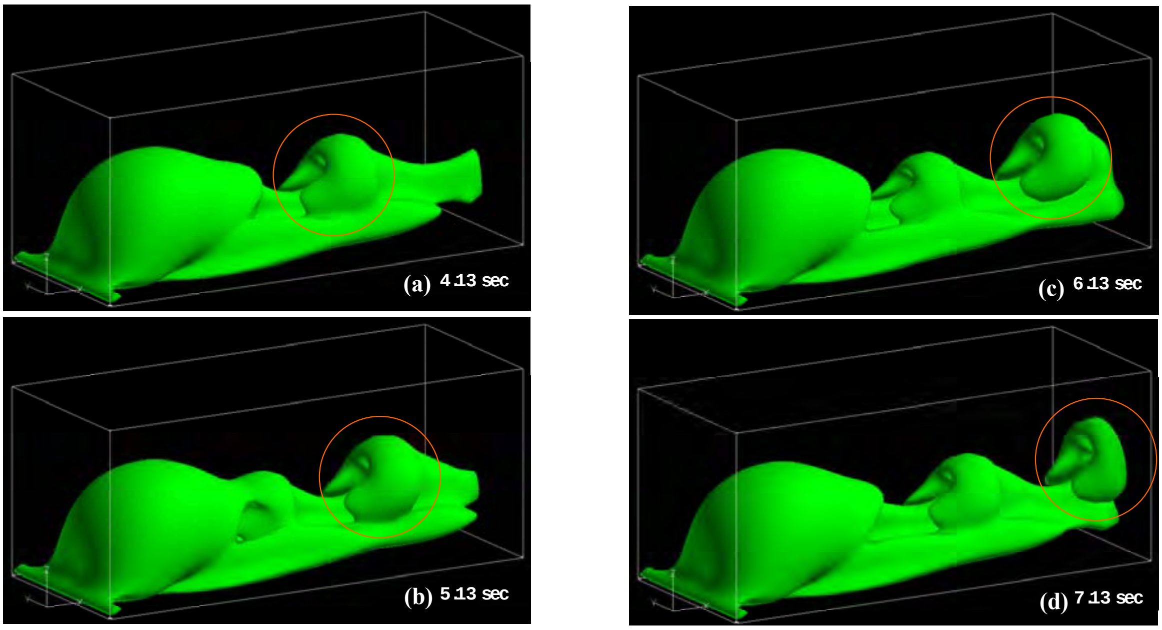


Fig. 7  Iso-surface transients of cross flow velocity components for the deflection jet case ($\beta$, Re) = (1.0, 600)

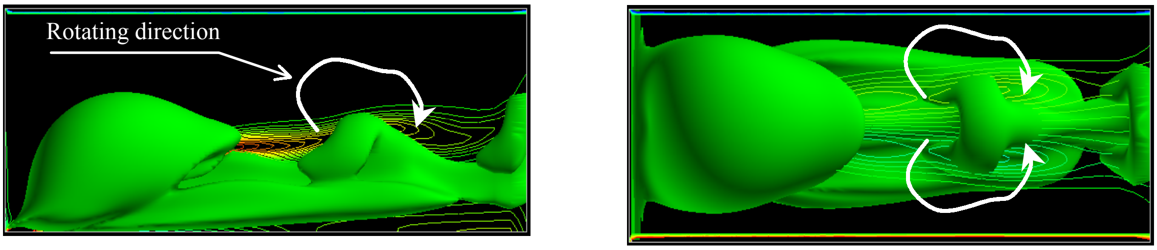


Fig. 8  Instantaneous distributions of iso-surface value of cross flow velocity and vorticities ($\beta$, Re) = (1.0, 600)

Figure 9 illustrates a detailed structure of the calculated arched vortex in the deflection jet condition (($\beta$, Re) = (1.0, 600)). As shown in the figure, the arched vortex consists of a head and two legs, together with a weak necklace vortex. The head of the arched vortex was affected by the main pipe flow shown by red region. On the other hand, the legs of the arched vortex were controlled by the branch pipe flow indicated by blue region. As for the necklace vortex, it was dominated by the main pipe flow.

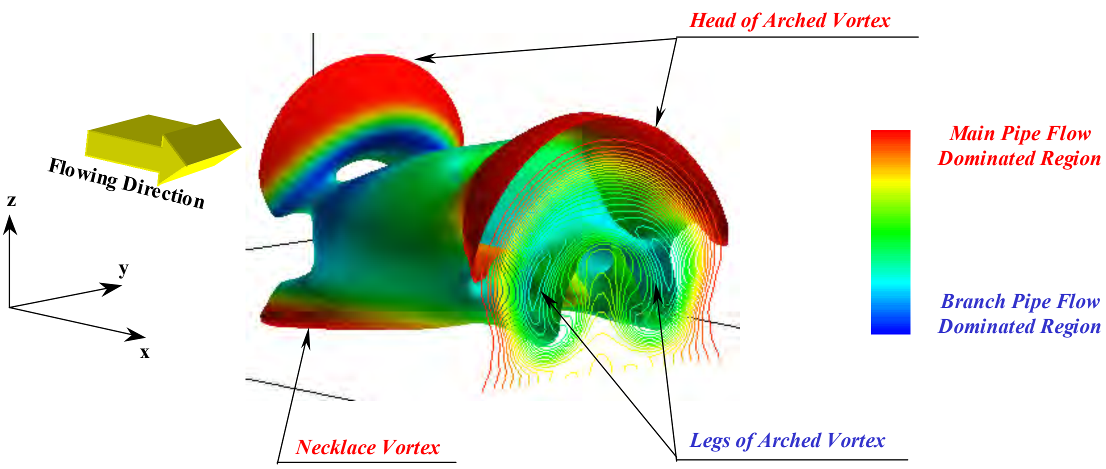


Fig. 9  Detailed structures of the arched vortex generated at ($\beta$, Re) = (1.0, 600) condition

An instantaneous pressure distribution around the arched vortices is drawn in Fig. 10 for the case of the deflection jet flows (($\beta$, Re) = (1.0, 600)). As shown in the figure, massive clouds of higher/lower pressures were generated in the main flow direction alternatively according to the presence of the heads of the arched vortices, and the internal pressure of the arched vortex head was decreased compared with the surrounding pressure of the arched vortex head. This fact supports that the arched vortex head is formulated by recirculation flows due to the vortex separation from the front of the branch pipe jet.

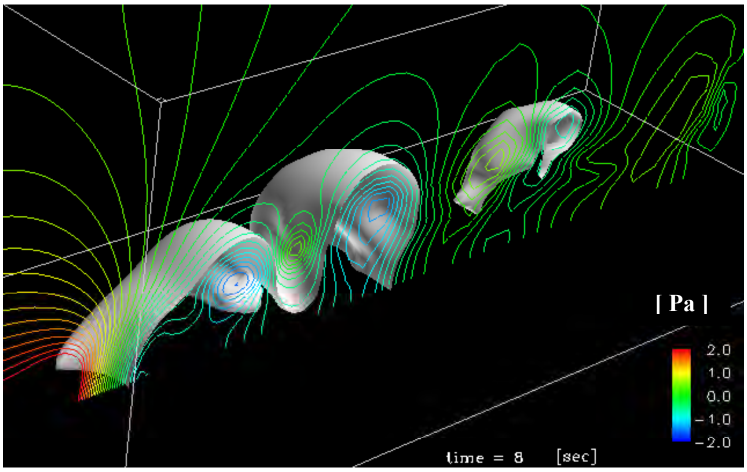


Fig. 10 Instantaneous pressure distribution around the arched vortices at ($\beta$, Re) = (1.0, 600) condition

Experimental results with respect to the generation frequency of the arched vortex were generalized as a function of $\alpha$, $\beta$ and Re. In this study, the generation frequency was defined by Strouhal number (St) using the following relationship:

$$\mathrm{St} = L / (U\,\tau), \qquad (4)$$

where

L = characteristics length (=B (9 mm)),

U = flow velocity in the rectangular main duct,

$\tau$ = generation period of the arched vortex ($f = 1/\tau$).

Figure 11 shows a comparison for the generation frequency of the arched vortex between experiments and calculations indicated by red star symbols. The experimental relationship indicated by a solid line in the figure is given by the following equation:

$$\mathrm{St} = 1.06\,(\alpha^{-1}\,\beta\,\mathrm{Re}^{\,0.2})^{-0.353}\,. \qquad (5)$$

As shown in this figure, the calculated results follow the experimental relationship very well and the figure shows good agreement of the calculated results with the experiments.

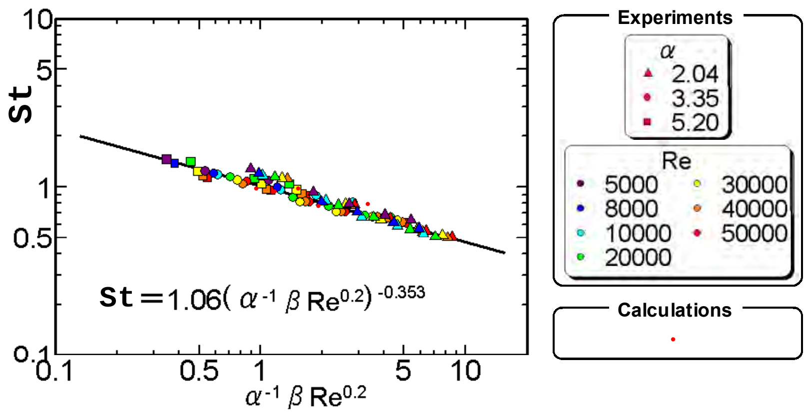


Fig. 11 Comparison of the generation frequency of the arched vortex

## 6. CONCLUSIONS

Thermohydraulic analyses for a fundamental water experiment simulating thermal striping at T-junction piping systems were carried out using a quasi-direct numerical simulation code DINUS-3. Calculated results were compared with the experimental results on the flow patterns in the downstream region of the T-junction piping systems, the arched vortex structures under the reflection jet condition, the generation frequency of the arched vortex, *etc*. in the various conditions; i.e., diameter ratio $\alpha$, flow velocity ratio $\beta$ and Reynolds number. From the comparisons, it was confirmed that (1) the DINUS-3 code is applicable to the flow pattern classifications in the downstream region of the T-junction piping systems, (2) the arched vortex characteristics with lower frequency components can be estimated numerically by the DINUS-3 code, and (3) special attentions should be paid to the arched vortex generations with lower frequency components of fluid temperature fluctuations, which might induced high-cycle thermal fatigue for the design of T-junction systems.

## REFERENCES


[1] Kasza, K. E. and Colwell, W. S., “Characterization of the Temperature Fluctuations Generated in a Thermal Mixing Tee”, *Proc of ANS / ASME / NRC Topical Meeting on Nuclear Reactors Thermal-Hydraulics*, Vol. 3, pp. 1852-1870, 1980.

[2] Wolf, L., Schygulla, U., Haffner, W., Fischer, K. and Baumann, W., “Results of Thermal Mixing Tests at the HDR-Facility and Comparisons with Best Estimate and Simple Codes”, *Nuclear Engineering and Design*, Vol. 99, No. 1, 1987, pp. 287-304.

[3] Simoneau, J. P, Noe, H. and Menant, B., “Large Eddy Simulation of Sodium Flow in a Tee Junction, -Comparison of Temperature Fluctuations with Experiments-“, *Pro. of 8th International Topical Meeting on Nuclear Reactor Thermal-Hydraulics*, Vol. 3, pp. 1404-1411, 1997.

[4] Muramatsu, T. and Ninokata, H., “Intensity Evaluation of the Temperature Fluctuations Related to Thermal Striping Phenomena Using the Algebraic Stress Turbulence Model”, *Proc. of ANS Winter Meeting*, pp. 156-162, 1991.

[5] Muramatsu, T. and Ninokata, H., “Thermal Striping Temperature Fluctuation Analysis Using the Algebraic Stress Turbulence Model in Water and Sodium”, *JSME International Journal*, Series II, Vol. 35. No. 4, pp, 1992, 486-496.

[6] Muramatsu, T., “Frequency Evaluation of Temperature Fluctuations Related to Thermal Striping Phenomena Using a Direct Numerical Simulation Code DINUS-3”, *Proc. of ASME Pressure Vessels and Piping Conference*, Vol. 253, pp. 111-121, 1993.

[7] Muramatsu, T., “Investigation of Sodium Temperature Fluctuation Characteristics Related to Thermal Striping Phenomena Using the DINUS-3 Code”, *Proc. of ASME Pressure Vessels and Piping Conference*, Vol. 270, pp. 23-27, 1994.

[8] Muramatsu, T., “A Direct Simulation Monte-Carlo Code THEMIS for the Evaluation of Nonstationary Heat Transfer Phenomena in LMFR Thermohydraulics”, *Proc. of 8th IAHR Working Group Meeting on Advanced Nuclear Reactors Thermal Hydraulics,* 1995.

[9] Muramatsu, T., “Thermal Response Evaluation of Austenitic Stainless Steels Due to Random Sodium Temperature Fluctuations Using BEMSET and DINUS-3 Codes”, *Proc. of ASME Pressure Vessels and Piping Conference*, Vol. 337, pp. 215-223, 1996.

[10] Iwata, K. and Tsukimori, K., “Extension of Finite Element Nonlinear Structural Analysis System FINAS Version 12.0”, *PNC Technical Report*, PNC TN9410 92-197, 1992.

[11] Watashi, K. and Yoshida, H., “CANIS Computer Code for Inelastic Fracture Mechanics”, *Proc. of ASME Pressure Vessels and Piping Conference*, Vol. 167, pp. 15-23, 1989.

[12] Muramatsu, T., “Numerical Analysis of Non-Stationary Thermal Response Characteristics for a Fluid-Structure Interaction System”, *Proc. of ASME Pressure Vessels and Piping Conference*, Vol. 363, pp. 149-156, 1998.

[13] Muramatsu, T., “Characteristics of Fluid - Structure Thermal Interaction Phenomena at a T-junction of Liquid Metal Fast Reactor Piping Systems”, *Proc. of 4th International Symposium on Computational Technologies for Fluid / Thermal / Chemical Systems with Industrial Applications*, Vol. 424-2, pp. 47-55, 2001.

[14] Sudo, K., Hibara, H. and Muramatsu, T., “Study on Turbulent Flows at a T-junction Piping System, -Characteristics of Flow Downstream from T-junction and Vortex Street Formed by Branch Pipe Flow”, *Proc. of JSME Annual Meeting*, Vol. II, pp. 191-192, 2001.

## APPENDIX : Phenomenology of thermal striping

Thermal striping phenomena are characterized by stationary random temperature fluctuations due to turbulence mixing processes. The fluid temperature fluctuations give generally high-cycle thermal fatigue to solid structures such as in-vessel components of LMFRs, T-junction piping systems, *etc.*. In the course of heat transfer including the temperature fluctuations to solid structures from fluids, there are significant attenuation mechanisms for the temperature fluctuation amplitudes indicated in Fig. A. 1. For the accurate evaluations of the thermal striping, three thermohydraulics computer programs and a thermomechanical computer program (see Fig. 1 and Table 1) were developed for the four attenuation mechanisms indicated in Fig. A. 1 (□, □, □and □).

Thermal striping analysis for an actual thermal fatigue event occurred at a French prototype LMFR PHENIX (Fig. A. 2) was carried out using the computer programs, in the framework of IAEA (International Atomic Energy Agency) coordinated research program (1996-1998) by Muramatsu (1999) and Kasahara (1999).

Figure A. 3 shows a calculated instantaneous circumferential sodium temperature distribution at 0.5 mm from the main pipe inner surface. As shown in the figure, thermally fluctuations were evaluated due to turbulence interactions between main pipe jet and branch jet. Furthermore cracked positions evaluated by fracture mechanics code based on the data of fluid-structure thermal interaction calculations agreed with actual positions shown in Fig. A. 2.

## REFERENCE IN APPENDIX


Muramatsu, T., “Evaluation of Thermal Striping Phenomena at a Tee Junction of LMFR Piping System with Numerical Methods (1), - Thermohydraulic Calculations –“, *Proc. of 15th International Conference on Structural Mechanics in Reactor Technology (SMiRT-15),* Vol. IV, pp. 217-224, 1999.

Kasahara, N., “Evaluation of Thermal Striping Phenomena at a Tee Junction of LMFR Piping System with Numerical Methods (2), - Thermomechanical Calculations –“, *Proc. of 15th International Conference on Structural Mechanics in Reactor Technology (SMiRT-15),* Vol. IV, pp. 209-216, 1999.


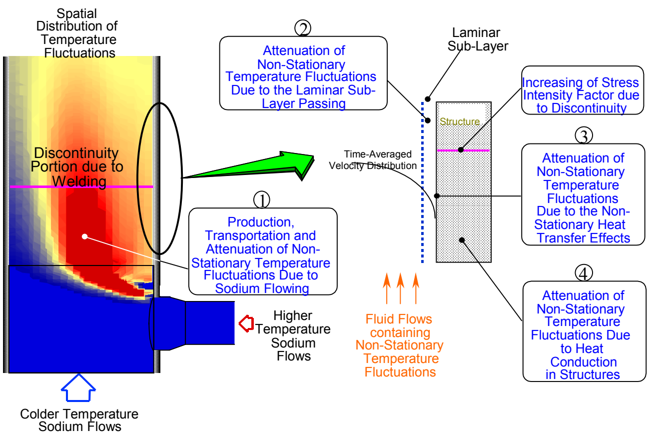


Fig. A. 1 Phenomenology of thermal striping and attenuation mechanisms of temperature fluctuation amplitudes

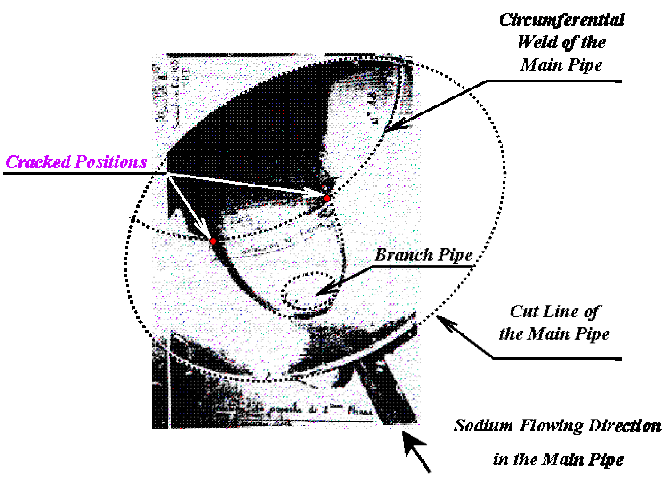


Fig. A. 2 Photograph of the investigated tee junction area of a French prototype LMFR PHENIX

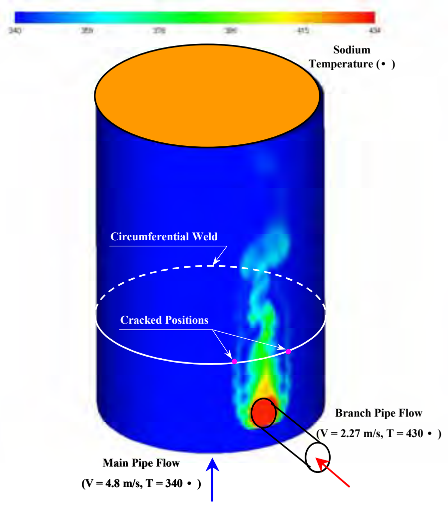


Fig. A. 3 Calculated instantaneous circumferential sodium temperature distributions at 0.5 mm from the main pipe inner surface